View Article Online / Journal Homepage / Table of Contents for this issue
Dynamic Article Links

Journal of Materials Chemistry

Cite this: J. Mater. Chem., 2012, 22, 23246

www.rsc.org/materials

PAPER

Single-step exfoliation and chemical functionalisation of graphene and *h*BN nanosheets with nickel phthalocyanine†

James Thompson,[a] Alison Crossley,[a] Peter D. Nellist[a] and Valeria Nicolosi*[b]

Received 23rd July 2012, Accepted 10th September 2012
DOI: 10.1039/c2jm34854c

Published on 11 September 2012. Downloaded by Trinity College Dublin on 28/03/2014 12:32:58.

Versatile routes to functionalise few-layer graphene and *h*BN with nickel phthalocyanine (Ni-Pc) were achieved using liquid phase exfoliation and sonication methods. EDX performed on the graphene//Ni-Pc specimen showed nickel on the flake surface whilst Raman spectroscopy revealed a prominent D peak indicating the presence of basal plane defects. New Raman active modes were also found in the *h*BN//Ni-Pc complex. X-ray photoelectron spectroscopy showed a charge transfer for both graphene and *h*BN confirming that the flake edges and basal-planes were covalently functionalised by the phthalocyanine molecules. Transmission electron microscopy confirmed the only presence of single and few-layer flakes of *h*BN and graphene in solution, demonstrating that the exfoliation yield was not affected by the functionalisation step. We therefore proved that tuning of the electronic and optical properties of graphene and *h*BN nanosheets is indeed conceivable. We used the Z-scan technique to prove the nonlinear optical (NLO) behaviour of the functionalised graphene sheets. Based on such optical response, we demonstrate an optical limiting effect for nanosecond laser pulses at 532 nm, proving these materials to be a suitable candidate for photonic and optoelectronic applications.

Introduction

Since its experimental discovery in 2004 (ref. 1) graphene has established itself as a viable candidate for replacing silicon technology and being used in the next generation of electronic devices. The sustained interest in graphene is due to its excellent electronic properties. It is a zero-gap semiconductor with its valence and conduction bands touching in *k*-space.[1] Graphene films show a strong ambipolar electric field effect where both electrons and holes can be the conducting entities.[1] Mobilities as high as 15 000 $cm^2 V^{-1} s^{-1}$ can be reached even at extremely high carrier concentrations.[1–4] The single and bi-layer forms are similar in that they are both zero-gap semiconductors with only a hole and an electron as charge carriers. For few-layer graphene a few more charge carriers appear as the valence and conduction bands begin to overlap, however, it can still be considered unique from the bulk material.[1,5] The 3D limit is at about 10 atomic layers.[6] Being a zero-gap semiconductor, a flat mono- or few-layer graphene is almost transparent and exhibits very low electrical resistivity at room temperature.[7] Electronics is where the majority of research is currently focussed, with graphene having promising applications in conducting films, FETs and logic gates in nanoelectronics as well as the potential in battery efficiency.[8] As an addition to graphene, a wide range of 2-dimensional (2-D) atomic crystals exist in nature, including transition metal dichalcogenides and hexagonal boron nitride (*h*BN) nanosheets.[9] The unique 2D structure of these materials gives rise to a variety of useful mechanical, optical and particularly electrical properties.[1,2,10]

The electronic structures of *h*BN and graphene are very different. The B–N bond shows some ionic character both in and out of the plane.[11] This polarity accounts for the different stacking sequence in BNNSs as well as slightly greater inter-layer forces. More importantly it means that, despite their similar crystal structure, *h*BN is an electrical insulator with a direct gap of about 5.8 eV.[12,13] Mechanically *h*BN sheets have been shown to be fairly strong; 1 nm thick BN sheets were found to have a breaking stress of 8.8 Nm^{-1} and a Young's modulus of 233 Nm^{-1} within the plane of the sheet.[13]

Potential applications are vast; the most immediate are likely to be in composites.[14] A likely application of pure *h*BN nanosheets is as a complementary dielectric to graphene in nanoelectronic devices, due to its large band gap.[15] Moreover, bulk *h*BN materials are currently used in a variety of diodes and other optoelectronic and electronic devices and the respective two-dimensional counterpart is expected to play a competing role in these types of applications.[16]

The scale investigation of these 2D nanomaterials has only recently become possible due to their increased availability through liquid phase exfoliation.[17,18] This process allows the quick and cheap high yield production of single layers of

[a]*Department of Materials, University of Oxford, Parks Road, OX1 3PH, Oxford, UK*
[b]*School of Chemistry, School of Physics & CRANN, Trinity College Dublin, Dublin 2, Ireland. E-mail: nicolov@tcd.ie; Tel: +353 (0)1 896 4408*

† Electronic supplementary information (ESI) available. See DOI: 10.1039/c2jm34854c

 This journal is © The Royal Society of Chemistry 2012

View Article Online

Published on 11 September 2012. Downloaded by Trinity College Dublin on 28/03/2014 12:32:58.

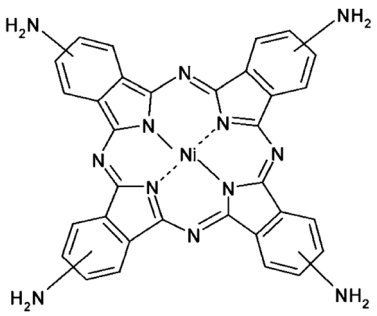

Fig. 1 Molecular structure of nickel(II) tetra-amino phthalocyanine.

virtually any inorganic layered material. These materials can be exfoliated as 2D nanosheets and used for the various different applications or added to other polymeric species or materials to produce composites.[17,18]

Graphene's transparency coupled with high mobility makes it an ideal candidate for the manufacturing of transparent conducting electrodes as a viable alternative to indium tin oxide (ITO).[19,20] However, recent results demonstrate that doping or chemical functionalisation are necessary steps to harvest the full potential of graphene.[20,21] On the other hand, the ability to tune the properties of *h*BN sheets by functionalising the surface would allow for the development of composite materials and interconnects for integrated nano-electronics. Functionalisation with specifically chosen molecules is a way to overcome many of the processing difficulties of these materials and tune them with respect to specific applications.[21,22] Hence research in this field is rapidly growing, with many methods being transferred from nanotubes to their 2D counterparts, where it is hoped the greater number of dangling bonds will increase the chances of a chemical interaction.

Herein we report for the first time a new method to directly alter the features of photochemically transparent graphene and *h*BN nanosheets by integrating a versatile electron donor system such as nickel phthalocyanines (structure in Fig. 1) in solution. Phthalocyanines are molecular semiconductors that have been shown to have interesting effects on the electrical and optical properties of multi-walled carbon nanotubes[23] and are expected to show similar, if not greater, effects on 2D nanomaterials.

We determine that the electrical and optical properties of 2D graphene and *h*BN nanosheets can be controlled by functionalisation with metal phthalocyanines and use a combination of UV-vis-NIR spectroscopy, Raman spectroscopy, X-ray photoelectron spectroscopy (XPS) and Energy-dispersive X-ray spectroscopy (EDX) to show the effect of functionalisation on the electronic structure as well as the likely physical structure. Transmission electron microscopy (TEM) is used to assess the flake quality, with the functionalised flakes compared to those produced previously by liquid phase exfoliation.

Experimental details

High quality graphene and *h*BN nanosheets were produced using the liquid phase exfoliation as described by Hernandez *et al.*[17] and Coleman *et al.*[18] respectively. Such mild strategies stand in strong contrast to other high-throughput techniques involving strong treatment of graphite with strong oxidants[23–25] or ionic intercalation,[26–28] where conversions (reduction of graphene oxide to obtain graphene or ionic de-intercalation) are by no means quantitative and results in irreversible re-aggregation and permanent lattice defects.[29,30]

Commercial graphite flakes or *h*BN powders were mixed with *N*-methyl-pyrrolidinone (NMP) with initial concentration of 1 g l^{-1} and sonicated for 1 hour in a low power sonic bath (Ultrawave U50 ultrasonic bath 100 W, 42 kHz) before being centrifuged at 1000 rpm for another hour. This results in a dark grey solution for graphene and a milky white solution for *h*BN.

The supernatant (top three quarters), which consisted solely of thin objects, was then decanted out using a pipette and transferred to a new vial. To include functionalisation in this process addition of the nickel phthalocyanine (Ni-Pc) powder to the solution is required. Functionalisation of the surface of the inorganic nanolayers will require an activation energy which can be supplied by sonication. Ni-Pc powders were therefore added to the exfoliated flakes in the supernatant in a 10 : 1 ratio by weight of exfoliated material/Ni-Pc. In order to do so an absorption spectrum was acquired from the originally decanted exfoliated supernatant and the concentration of the dispersion was calculated using Beer–Lambert law. The mass of flakes was then calculated, and 1/10th of this mass of Ni-Pc is added to the vial in solution.

This was followed by re-sonication in a low power sonic bath (Ultrawave U50 ultrasonic bath 100 W, 42 kHz) for another hour. It is very important to notice that a different preparation procedure consisting of one single step was also investigated. This involved mixing raw Ni-Pc and graphite powders together in a ratio 1 : 10 by weight. NMP was successively added to achieve an initial graphite concentration of 1 g l^{-1}. This was

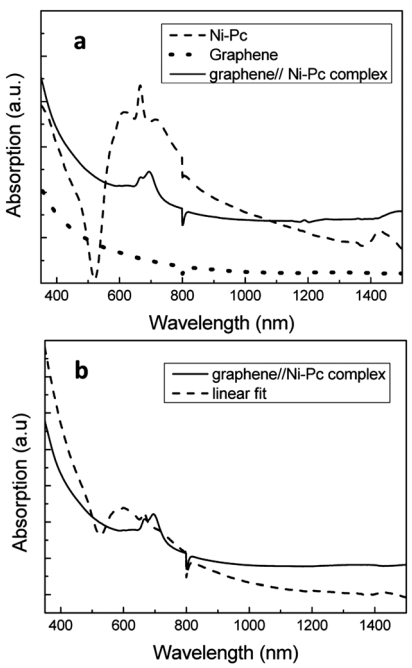

Fig. 2 Absorption spectra of: (a) as-exfoliated graphene (dotted line), as-dispersed Ni-Pc (dashed line) and the graphene//Ni-Pc complex (continuous line) and (b) the graphene//Ni-Pc complex (continuous line) and linear fit (dashed line) showing new peaks in the Ni-Pc/graphene absorption spectrum.

View Article Online

Published on 11 September 2012. Downloaded by Trinity College Dublin on 28/03/2014 12:32:58.

followed by bath sonication for 1 hour and centrifugation at 1000 rpm for another hour. It is, however, important to notice that the one-step preparation just described did not lead to any functionalisation evidence as shown in the ESI†.

UV-vis-NIR absorption spectra were acquired using a Varian Cary 5000 Spectrometer (scan rate = 600 nm min) using 1 cm optical glass cuvettes. Spectra were background corrected and acquired in a range of wavelengths going from 200 to 2100 nm.

Spectra of the nanosheets//Ni-Pc complex were fitted using a linear combination of the absorption spectra acquired independently for graphene/*h*BN and Ni-Pc dispersions prepared under comparable processing conditions. This was done using a basic trial and error addition method by altering the linear coefficients and served as a rough guide to see if any spectral shift or new feature was originated in the complex. Raman spectroscopy was carried out using a LabRAM Aramis (solid state laser at 532 nm). A few drops of each sample were drop-cast onto silicon wafers and the solvent allowed to evaporate. For each sample Raman shifts were acquired in the range of 500–3500 cm^{-1} and averaged over at least 4 sample spots. XPS was performed using an ion pumped VG Microtech CLAM 4 MCD analyser system. Samples for XPS were deposited onto a silicon substrate and the remaining solvent evaporated. The specimens were irradiated with 200 Watt Mg X-rays (un-monochromated). For wide scans the analyser was operated at a constant pass energy of 100 eV with 1 eV steps, for detailed scans a constant pass energy of 20 eV with 0.1 eV steps was used. All spectra had the C1s peak corrected to 248.8 eV to account for any sample charging. A Shirley background subtraction was used. TEM images were recorded using a JEOL 2010 or a JEOL 2000FX operated at 200 kV TEM. HRTEM images and EDX spectra were recorded using a JEOL 3000F equipped with an Oxford Instruments INCA detector and operated at 300 kV. Samples for TEM were drop-cast onto lacy carbon 400 mesh. Low resolution images of the objects were taken in a bright-field diffraction contrast mode, while HRTEM images were recorded in phase-contrast mode. Z-scan nonlinear optical measurements on functionalised and unfunctionalised graphene dispersions were performed with an open-aperture set-up, using an incident energy of 532 nm.

Results and discussion

Graphene

Absorption spectroscopy was used to look for changes in the optical behaviour of the mixtures (Fig. 2a). The spectrum of as-exfoliated graphene is as expected relatively featureless with some absorption at low wavelengths. The Ni-Pc spectrum shows two main absorption regions. At wavelengths between 250 and 500 nm there is absorption due to $\pi \rightarrow$ d transitions involving the central metal ion, this is known as the Soret band or B band.[31,32] The absorption region centred on 650 nm is due to $\pi \rightarrow \pi^*$ transitions from overlapping π-orbitals and is known as the Q band.[31,32] The Q band shows Davydov splitting resulting in the peak at 670 nm. The spectrum relative to the graphene//Ni-Pc complex showed the presence of a new peak at 702 nm. It was not possible to perform a linear fit on this curve (Fig. 2b). This suggests an alteration of the electronic and optical properties in the sample due to the presence of chemical interactions between the graphene and the nickel phthalocyanine molecules.

It is critical to determine the exfoliation state of the graphene// Ni-Pc in these dispersions. To do so we performed TEM analysis on our dispersions, typically solely observing 2-dimensional flakes consisting of single or few-layer nanosheets. Examples of very thin sheets observed in our dispersions are shown in Fig. 3a and b. The addition of Ni-Pc did not appear to have affected the exfoliation process significantly, nor did it lead to excessive re-aggregation of the flakes. The TEM lacey carbon support resulted free from any large Ni-Pc aggregate, suggesting uniform interaction of the phthalocyanine molecules at the graphene's surface and edges. The lateral size of these objects was typically 500–1000 nm (see Fig. 3c and d for statistics). This is comparable to flake sizes obtained for as-exfoliated graphene reported elsewhere.[17]

So far we have confirmation of an alteration of the optical response in the graphene//Pc dispersion as compared to the two as-dispersed raw materials and TEM evidence for high yield and good quality graphene exfoliation. Furthermore we observe that Ni-Pc molecules do not cluster on the TEM support to give large phthalocyanine aggregates. A TEM image of a typical large aggregate obtained dispersing Ni-Pc powders in NMP and the relative EDX spectrum are shown in the ESI† for completeness. However, we have no confirmation of the actual presence of Ni-Pc on the graphene sheets either. In order to investigate this further EDX spectroscopy was employed to analyse qualitatively the chemical nature of the obtained graphene//Ni-Pc flakes. A typical EDX spectrum acquired on one of the graphene//Ni-Pc flakes is shown in Fig. 4. A significant number of counts is detected at 7.6 keV indicating the presence of small amounts of nickel at the surface of the nanosheets (Fig. 4). The spectrum also shows an iron signal originating from the TEM objective lens (iron Kα and Kβ peaks at 6.4 keV and 7.06 keV respectively) and

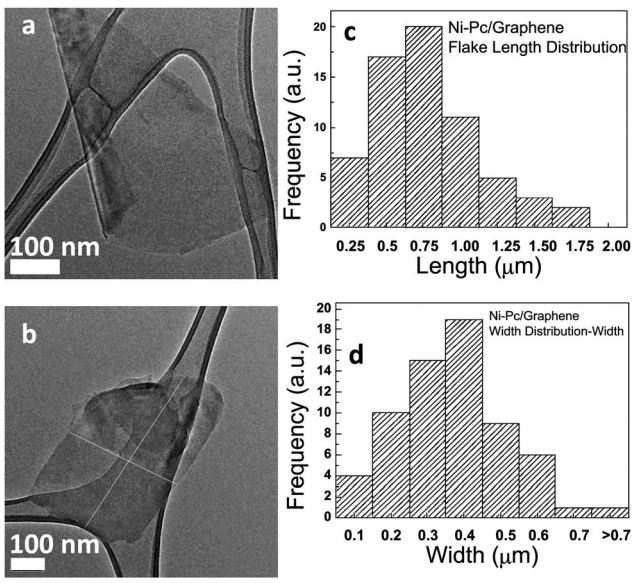

Fig. 3 TEM diffraction contrast images of (a) a thin flake typically found in the graphene//Ni-Pc specimen; (b) flake showing how the size measurements were taken. (c) and (d) Histograms showing length and width statistics.

 This journal is © The Royal Society of Chemistry 2012

View Article Online

Published on 11 September 2012. Downloaded by Trinity College Dublin on 28/03/2014 12:32:58.

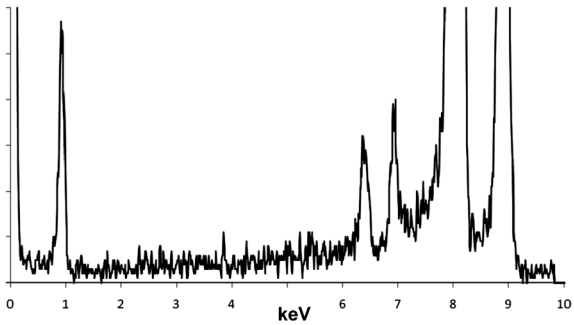

Fig. 4 EDX spectrum of the Ni-Pc/graphene flake surface showing a small Ni signal at 7.6 keV.

a copper contribution (copper Kα at 8.046 eV and Kβ at 8.904 keV) from the support grid. In spite of a detectable contribution from the nickel species, we must underline the qualitative nature of the EDX information.

Raman spectroscopy was therefore used to obtain structural information appearing in the Raman-active low frequency modes. Raman spectroscopy of graphene has been well studied and can give information on the number and orientation of atomic layers as well as the presence of doping and defects.[17] The two most intense features seen in all graphene/graphite Raman spectra are the G peak at ~1580 cm^{-1} and the 2D peak at ~2700 cm^{-1} (ref. 33 and 34) (Fig. 5a). The G peak corresponds to the doubly degenerate E_{2g} phonon at the Brillouin zone centre.[33] The intensity of the G peak is independent of the number of graphene layers, but will shift to higher wavenumbers (about 3–5 cm^{-1} ref. 34) when going from bulk graphite to graphene. The 2D peak is the second order peak of TO zone boundary phonons (due to the breathing modes of sp^2 atoms).[17,35–37] This is a single sharp peak in a single layer graphene which splits into 4 peaks for the bi-layer graphene. Increasing the number of layers shifts this peak up in wavelength as well as resolving into a broader curve than a single sharp peak.[34] The intensity of this peak will be four times greater than the G peak for the single layer graphene, however, for bulk graphite it will be only roughly one third as intense as the G peak. The first order zone boundary phonons are only seen in defective graphite.[17] They give rise to the D peak at ~1350 cm^{-1} which can be seen in single/bi-layer graphene.[33] It is normally only detectable at the edge of a flake due to a higher concentration of defects. The intensity of this peak rapidly diminishes with increasing numbers of atomic layers. In a single layer its intensity will be roughly 1/5th that of the G band and will decrease exponentially with increasing number of layers.[33] Phthalocyanines have again been well studied due to their common use in dyes and pigments. A_{1g}, B_{1g}, B_{2g} and E_g modes are Raman active and hence there are many peaks in the spectra in the region 500–2000 cm^{-1} (Fig. 5b).

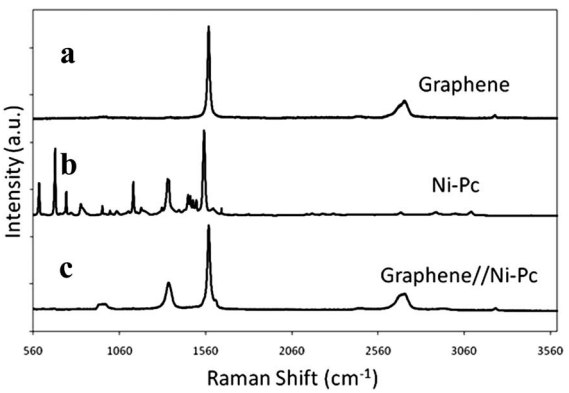

Fig. 5 Comparison of Raman spectra for Ni-Pc/graphene.

The region from 1300 to 1600 cm^{-1} is known as the 'fingerprint region' as it is unique for each metallo-phthalocyanine. The major peak in this region is at 1545 cm^{-1} and is due to the nickel atom in the centre of the macrocyclic ring. It is the largest of any metallo-phthalocyanine due to the distorted macromolecule. As the nickel ion is essentially 'too small' for the hole, the C–N–C bridge bonds will deform and stretch to accommodate it. In comparison, Raman spectra of the graphene//Ni-Pc complex showed clear 2D and G peaks, ultimately indicating graphene flakes consisting of few layers (Fig. 5c). Not surprisingly, rather than having a simple added contribution from the Ni-Pc spectrum we can now distinguish features previously not observed in the as-exfoliated graphene and dispersed Ni-Pc. A very sharp D peak at 1340 cm^{-1} and a small, broad peak in the region 930–950 cm^{-1} are now present in the spectrum of the graphene//Ni-Pc complex.

The existence of a D band is usually associated with the presence of finite crystal sizes or distortion/defects in the lattice provoking alteration of the electronic structure at the Brillouin-zone boundary. This contribution was not present in the unfunctionalised graphene, suggesting that the addition of the Ni-Pc domain has an effect on the local bonding, generating remarkable disorder in the graphene's sp^2 hybridized lattice. However, it is important to notice that D peaks are usually smaller than the 2D, while in our case it is roughly 50% more intense. Similarly, works on graphene functionalised by 1,3-dipolar cycloaddition[38] also reported the appearance of intense D peaks upon functionalisation and attributed it to the formation of basal plane defects generated by the attachment of the functional groups. Further work on functionalisation of graphene oxide also showed a similarly prominent D peak.[39] This was again attributed to the presence of structural basal plane imperfections. We can rule out the possibility of having oxidised the surface for several reasons; firstly the lack of a prominent D peak in the spectra of pure graphene prepared under identical conditions and secondly the lack of detectable oxygen content in the XPS (not shown). The existence of a peak at 930–945 cm^{-1} was never previously reported in the literature for either functionalised or unfunctionalised graphene. This suggests the presence of new Raman active modes in the graphene//Ni-Pc complex.

Whereas Raman spectroscopy was adequate to reveal the presence of a strongly active D mode in the functionalised sample, we still lack the key information on whether the Ni-Pc is bonded to the graphene. XPS was therefore used to obtain crucial information on the electronic state of the different chemical groups present. Any change in the electronic state of the species contained in the phthalocyanine molecules would provide strong evidence of a charge transfer between these and the graphene layers. We expect this transfer to occur through the central nickel atom due to the high charge density at the phthalocyanine core, meaning that the Pc molecule would lie parallel to the

View Article Online

Published on 11 September 2012. Downloaded by Trinity College Dublin on 28/03/2014 12:32:58.

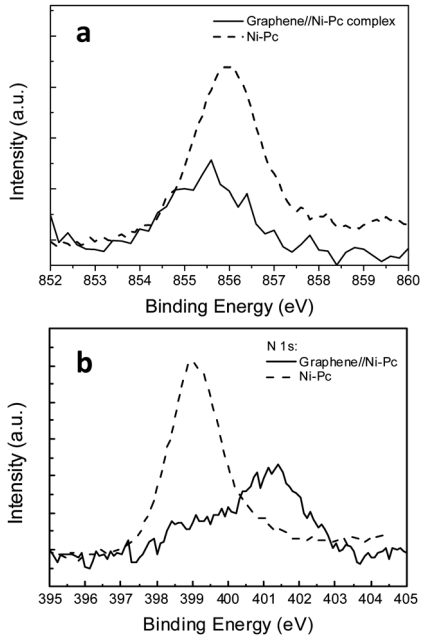

Fig. 6 XPS spectra for Ni-Pc (dashed line) and the graphene//Ni-Pc complex (continuous line): (a) Ni $2p_{3/2}$ and (b) N 1s.

graphene surface. XPS spectra were acquired for graphene, Ni-Pc and the Ni-Pc/graphene complex (Fig. 6). None of these showed effects of charging meaning that minimal correction was required during acquisition and post-processing. A detailed comparison of binding energies (E_b) for nickel and nitrogen species in pure Ni-Pc and graphene//Ni-Pc complexes is shown in Fig. 6a and b respectively. The detection of the Ni $2p_{3/2}$ signal in the graphene//Ni-Pc complex was significative of the presence of phthalocyanines lying on the graphene's flake surface. Even more important to notice is the blueshift of the binding energies associated with both nickel $2p_{3/2}$ and nitrogen 1s in the complex. This can be interpreted as an increase in the nickel electron density, consequence of a charge transfer from the graphene onto the phthalocyanine molecule.

Finally, we performed HRTEM on typical unfunctionalised (Fig. 7a) and functionalised graphene//Ni-Pc flakes (Fig. 7b). This confirms that the crystal structure of the material has not been compromised by the functionalization process. Impurities, holes or eventual defects are not observable in the two samples demonstrating only good quality nanosheets.

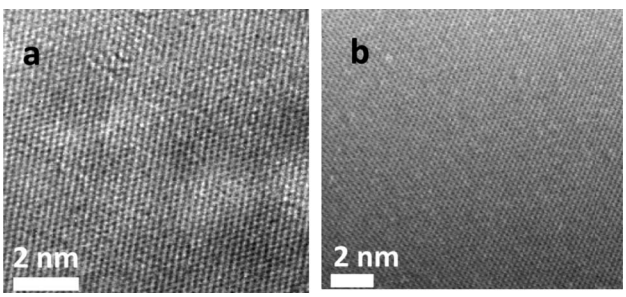

Fig. 7 HRTEM images of: (a) as-exfoliated graphene and (b) the graphene//Ni-Pc complex.

The ultimate optical performance of the functionalised graphene systems was validated by performing nonlinear optical measurements by Z-scan. In this work, an open-aperture Z-scan system is used to study the NLO behaviour of functionalised and unfunctionalised graphene, as well as of the as-dispersed Ni-Pc. This measured the total transmittance through a sample as a function of incident laser intensity, while the sample is gradually moved along the z-axis, through the focus of a lens. Fig. 8 shows the variation for the different dispersions of the normalised transmission as a function of the incident pulse-energy density (J cm^{-2}) when excited by a nanosecond laser at 532 nm.

All dispersions show a gradually reduced transmission with increasing incident energy indicating a clear optical limiting effect. The functionalised graphene//Ni-Pc sample shows the biggest effect strongly attenuating the intense and potentially dangerous laser beam, while exhibiting high transmittance for the low-intensity ambient light. This effect makes this material particularly useful and particularly promising.

h-Boron nitride

High-quality *h*BN flakes were produced by means of solution processing, which involves exfoliating and dispersing them directly from the bulk *h*BN material, as discussed in the Experimental details. Optical absorption spectroscopy of the as-exfoliated materials appears to be relatively featureless (Fig. 9a).

When Ni-Pc was introduced in the system according to the method described in the Experimental details, it causes a modification of the UV-vis spectrum, which leads to the appearance of a new feature centred at about 614 nm (Fig. 9a). The Ni-Pc spectrum exhibits a broad and strong absorption in that region. However, a closer look and an attempt to fit the *h*BN//Ni-Pc curve using a linear combination of the absorption spectra of similarly prepared *h*BN and Ni-Pc dispersions reveals substantial differences (Fig. 9b). This reflects the presence of strong electronic coupling between the individual components in the *h*BN//Ni-Pc complex.

Transmission electron microscopy was used to investigate the morphological properties of the *h*BN//Ni-Pc complex, showing very high yield of exfoliated, only few-layer thick flakes (Fig. 10). This confirmed that exfoliation in the presence of Ni-Pc

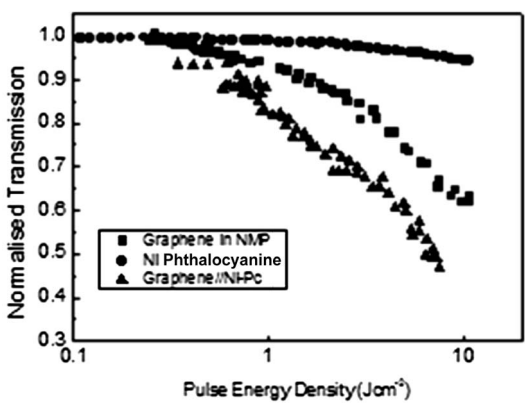

Fig. 8 Nonlinear transmission of: graphene in NMP (squares), Ni-Pc in NMP (circles) and graphene//Ni-Pc in NMP (triangles) for a laser excitation of 532 nm.

 This journal is © The Royal Society of Chemistry 2012

View Article Online

Published on 11 September 2012. Downloaded by Trinity College Dublin on 28/03/2014 12:32:58.

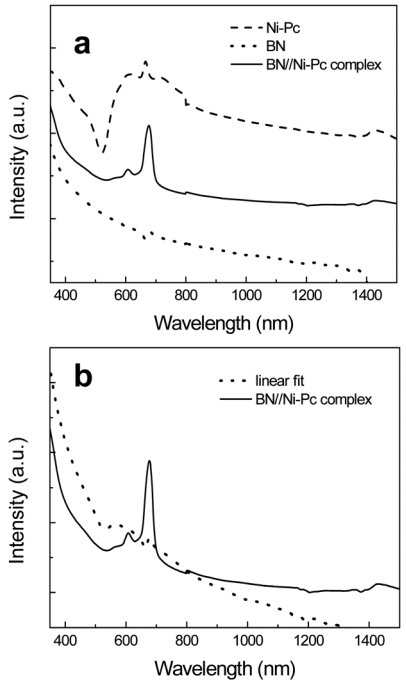

Fig. 9 Absorption spectra of: (a) as-exfoliated graphene (dotted line), as-dispersed Ni-Pc (dashed line) and the graphene//Ni-Pc complex (continuous line) and (b) best linear fit showing new peaks appearing in the Ni-Pc/BN absorption spectrum.

molecules had not effected the overall quality of the nanosheets in the complex. Only minimal re-aggregation seemed to have occurred in either sample, with the vast majority of flakes appearing thin and well separated in the grid.

Two distinct flake morphologies were overall observed: angular edges and corners (Fig. 10a) and circularly shaped sheets (Fig. 10b). Flake size statistical analysis for the two different sheet geometries revealed normal distributions (Fig. 10c and d), with average flake sizes (0.705 ± 0.0978 μm by 0.462 ± 0.0536 μm) comparable to unfunctionalised, exfoliated flakes

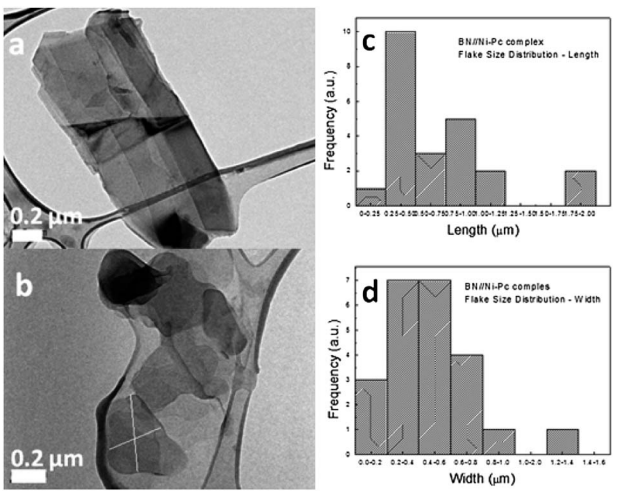

Fig. 10 TEM diffraction contrast images of typical functionalised *h*BN flakes: (a) a thin flake with angular morphology and (b) a thin flake with circular morphology showing how the size measurements were taken. (c) and (d) Histograms showing length and width statistics.

reported elsewhere.[19] It is particularly important to notice that no residual Ni-Pc aggregates were found on the TEM support.

Raman spectroscopy was once again used to gather structural information from the active low frequency modes. Bulk *h*BN has a main Raman line at 1366 cm^{-1} and a very low intensity line at 52.5 cm^{-1} that cannot always be measured.[39] The 1366 cm^{-1} peak arises from a mode that can be constructed *via* zone folding of the Raman active E_{2g} mode. This mode undergoes an up-shift and broadening for smaller *h*BN crystallites.[40]

Overall the detailed interpretation of the spectra proved to be rather challenging. Previous Raman studies on *h*BN looked either at the bulk material[40,41] or at nanotubes[40] which may have different features if compared to the few-layer *h*BN investigated here. Furthermore literature presents many reports where theoretical studies[43] are in conflict with experimental ones.[44,45] Our primary scope in this work is to compare the Raman spectra of the *h*BN//Ni-Pc nanosheets with those of the pure materials and to highlight the generated diversities induced by the functionalisation process. Typical Raman spectra for the complex and the two as-dispersed raw materials are shown in Fig. 11a.

A comparison study leads to the conclusion that the Ni-Pc modes in the spectrum of the *h*BN//Ni-Pc complex are much weaker if compared to the pure phthalocyanines. Moreover, a new and very broad peak can be detected at 2700 cm^{-1}(Fig. 11a). This is very similar to the 2D peak found in few-layer graphene samples. It is particularly interesting to notice that this peak was not found in any of the pure *h*BN spectra. A direct comparison of the phthalocyanine 'fingerprint' region (Fig. 11b) also shows that the dispersed Ni-Pc and the *h*BN//Ni-Pc complex are not a direct match. Whilst not being as conclusive as for the graphene complex, Raman spectroscopy clearly shows a remarkable change in the behaviour of the low-frequency modes. These

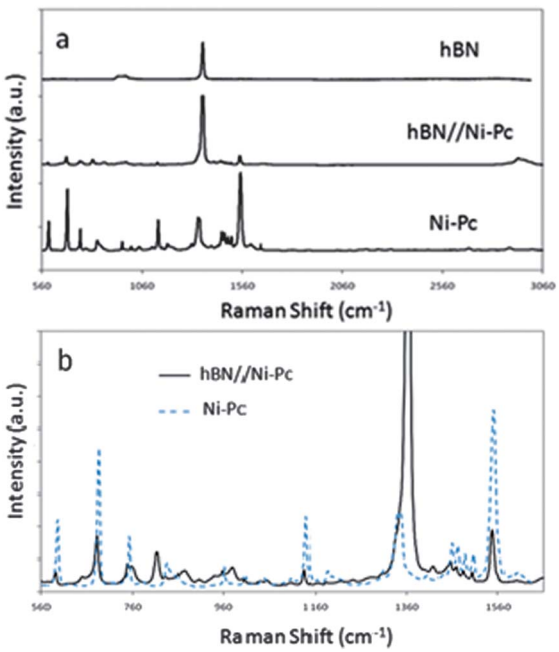

Fig. 11 Comparison of Raman spectra of: (a) as-exfoliated *h*BN, as-dispersed Ni-Pc and the Ni-Pc//*h*BN complex and (b) the fingerprint region of as-dispersed Ni-Pc and the Ni-Pc//*h*BN complex.

View Article Online

Published on 11 September 2012. Downloaded by Trinity College Dublin on 28/03/2014 12:32:58.

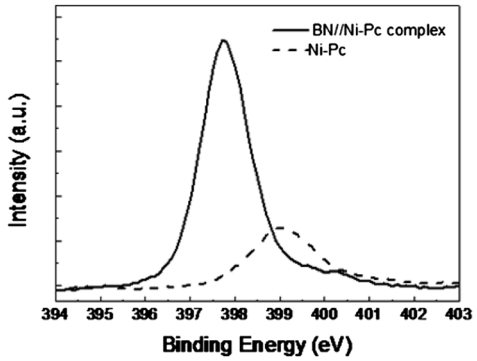

Fig. 12 N 1s XPS spectra for Ni-Pc (dotted line) and the *h*BN//Ni-Pc complex (continuous line).

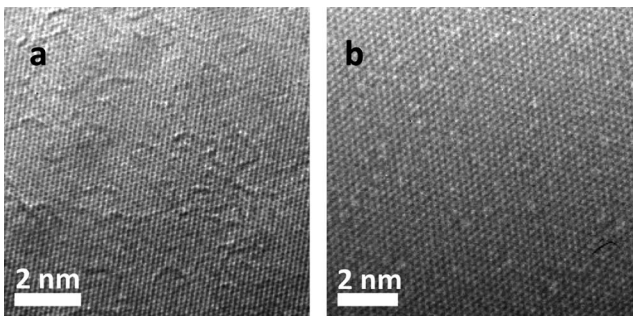

Fig. 13 HRTEM images of: (a) as-exfoliated graphene and (b) the graphene//Ni-Pc complex.

differences are sufficiently significant to suggest efficient functionalisation. Further insights came from the XPS analysis.

Given the very low content of phthalocyanines in the complex, it was not possible to detect any nickel contribution to the spectrum. The presence of the phthalocyanine in the complex was nevertheless detectable from the signal associated with the four pyrrole nitrogen atoms, the next four closest atoms to the centre of the phthalocyanine molecule. A direct comparison of the nitrogen 1s binding energy of pure phthalocyanine and *h*BN//Ni-Pc samples (Fig. 12) reveals a blueshift of 0.7 eV in the functionalised sample, which is a proof of unambiguous charge transfer from the phthalocyanine onto the *h*BN sheet.

Lastly, in order to verify the quality of the functionalised sample we performed HRTEM on typical unfunctionalised *h*BN (Fig. 13a) and functionalised *h*BN//Ni-Pc nanosheets (Fig. 13b).

The good quality (absence of large aggregates, defects or impurities) on the surface demonstrates that the functionalization process is not invasive. This is highly desirable to retain the intrinsic properties of the *h*-BN sheets.

Conclusions

In conclusion we have presented a facile, cheap and easily scalable route for the functionalisation of graphene and *h*BN nanosheets with Ni-Pc in solution. In both cases we obtained very stable dispersions with high concentrations of high-quality mono- and few-layer graphene and *h*BN sheets. The results for *h*BN sheets run almost in parallel to those for graphene. Both the exfoliated graphene//Ni-Pc and the *h*BN//Ni-Pc complexes give rise to strong electronic coupling between the individual components giving rise to new fingerprint optical absorptions. EDX corroborated the presence of nickel species in the functionalised nanosheets, while Raman showed that functionalisation occurs causing prominent basal plane defects generated by the attachment of the functional groups. XPS measurements confirmed that the nature of these interactions is electron transfer from Ni-Pc to *h*BN and from graphene to Ni-Pc respectively. Therefore we proved that tuning of the electronic and optical properties of graphene and *h*BN is indeed conceivable.

Acknowledgements

VN wishes to thank the European Research Council for funding through the grant 2DNanoCaps. The authors thank BeggbrokeNano for their provision of research facilities.

Notes and references

1 K. S. Novoselov, A. K. Geim, S. V. Morozov, D. Jiang, Y. Zhang, S. V. Dubonos, I. V. Grigorieva and A. A. Firsov, *Science*, 2004, **306**, 666–669.
2 K. S. Novoselov, D. Jiang, F. Schedin, T. J. Booth, V. V. Khotkevich, S. V. Morozov and A. K. Geim, *Proc. Natl. Acad. Sci. U. S. A.*, 2005, **102**, 10451–10453.
3 Y. B. Zhang, Y. W. Tan, H. L. Stormer and P. Kim, *Nature*, 2005, **438**, 201–204.
4 K. S. Novoselov, A. K. Geim, S. V. Morozov, D. Jiang, M. I. Katsnelson, I. V. Grigorieva, S. V. Dubonos and A. A. Firsov, *Nature*, 2005, **438**, 197–200.
5 S. V. Morozov, K. S. Novoselov, F. Schedin, D. Jiang, A. A. Firsov and A. K. Geim, *Phys. Rev. B: Condens. Matter Mater. Phys.*, 2005, **72**, 201401–1.
6 B. Partoens and F. M. Peeters, *Phys. Rev. B: Condens. Matter Mater. Phys.*, 2006, **74**, 193402–1.
7 M. S. Fuhrer and S. Adam, *Nature*, 2009, **458**, 38.
8 A. K. Geim and K. S. Novoselov, *Nat. Mater.*, 2007, **6**, 183–191.
9 K. S. Novoselov, D. Jiang, F. Schedin, T. J. Booth, V. V. Khotkevich, S. V. Morozov and A. K. Geim, *Proc. Natl. Acad. Sci. U. S. A.*, 2005, **102**, 10451–10453.
10 C. Oriakhi and M. Lerner, in *Handbook of Layered Materials*, CRC Press, 2004.
11 D. Golberg, Y. Bando, Y. Huang, T. Terao, M. Mitome, C. C. Tang and C. Y. Zhi, *ACS Nano*, 2010, **4**, 2979–2993.
12 D. Golberg, Y. Bando, Y. Huang, Z. Xu, X. L. Wei, L. Bourgeois, M. S. Wang, H. B. Zeng, J. Lin and C. Y. Zhi, *Isr. J. Chem.*, 2010, **50**, 405–416.
13 L. Song, L. Ci, H. Lu, P. B. Sorokin, C. Jin, J. Ni, A. G. Kvashnin, D. G. Kvashnin, J. Lou, B. I. Yakobson and P. M. Ajayan, *Nano Lett.*, 2010, **10**, 3209–3215.
14 S. Stankovich, D. A. Dikin, G. H. B. Dommett, K. M. Kohlhaas, E. J. Zimney, E. A. Stach, R. D. Piner, S. T. Nguyen and R. S. Ruoff, *Nature*, 2006, **442**, 282–286.
15 C. R. Dean, A. F. Young, I. Meric, C. Lee, L. Wang, S. Sorgenfrei, K. Watanabe, T. Taniguchi, P. Kim, K. L. Shepard and J. Hone, *Nat. Nanotechnol.*, 2010, **5**, 722–726.
16 C. Y. Zhi, Y. Bando, C. C. Tang, H. Kuwahara and D. Golberg, *Adv. Mater.*, 2009, **21**, 2889.
17 Y. Hernandez, V. Nicolosi, M. Lotya, F. M. Blighe, Z. Y. Sun, S. De, I. T. McGovern, B. Holland, M. Byrne, Y. K. Gun'ko, J. J. Boland, P. Niraj, G. Duesberg, S. Krishnamurthy, R. Goodhue, J. Hutchison, V. Scardaci, A. C. Ferrari and J. N. Coleman, *Nat. Nanotechnol.*, 2008, **3**, 563–568.
18 J. N. Coleman, M. Lotya, A. O'Neill, S. D. Bergin, P. J. King, U. Khan, K. Young, A. Gaucher, S. De, R. J. Smith, I. V. Shvets, S. K. Arora, G. Stanton, H. Y. Kim, K. Lee, G. T. Kim, G. S. Duesberg, T. Hallam, J. J. Boland, J. J. Wang, J. F. Donegan, J. C. Grunlan, G. Moriarty, A. Shmeliov, R. J. Nicholls, J. M. Perkins, E. M. Grieveson, K. Theuwissen,

 This journal is © The Royal Society of Chemistry 2012

View Article Online

D. W. McComb, P. D. Nellist and V. Nicolosi, *Science*, 2011, **331**, 568–571.
19 G. Eda, G. Fanchini and M. Chhowalla, *Nat. Nanotechnol.*, 2008, **3**, 270.
20 S. De and J. N. Coleman, *ACS Nano*, 2010, **4**, 2713.
21 D. Pacile, J. C. Meyer, C. O. Girit and A. Zettl, *Appl. Phys. Lett.*, 2008, **92**, 3.
22 M. Giovanni, H. L. Poh, A. Ambrosi, G. Zhao, Z. Sofer, F. Šaněk, B. Khezri, R. D. Webster and M. Pumera, *Nanoscale*, 2012, **4**, 5002–5008.
23 A. T. Chidembo, K. I. Ozoemena, B. O. Agboola, V. Gupta, G. G. Wildgoose and R. G. Compton, *Energy Environ. Sci.*, 2010, **3**, 228–236.
24 W. S. Hummers and R. E. Offeman, *J. Am. Chem. Soc.*, 1958, **80**, 1339.
25 B. Brodie, *Ann. Chim. Phys.*, 1860, **59**, 466.
26 L. Staudenmaier, *Ber. Dtsch. Chem. Ges.*, 1898, **31**, 1481.
27 R. Bissessur, M. G. Kanatzidis, J. L. Schindler and C. R. Kannewurf, *J. Chem. Soc., Chem. Commun.*, 1993, 1582.
28 G. L. Frey, K. J. Reynolds, R. H. Friend, H. Cohen and Y. Feldman, *J. Am. Chem. Soc.*, 2003, **125**, 5998.
29 R. A. Gordon, D. Yang, E. D. Crozier, D. T. Jiang and R. F. Frindt, *Phys. Rev. B: Condens. Matter Mater. Phys.*, 2002, **65**, 125407–1.
30 I. Jung, D. Dikin, R. Piner and R. Ruoff, *Nano Lett.*, 2008, **8**, 4283.
31 D. R. Tackley, G. Dent and W. E. Smith, *Phys. Chem. Chem. Phys.*, 2001, **3**, 1419–1426.
32 K. N. N. Unni and C. S. Menon, *Mater. Lett.*, 2000, **45**, 326–330.
33 A. C. Ferrari, J. C. Meyer, V. Scardaci, C. Casiraghi, M. Lazzeri, F. Mauri, S. Piscanec, D. Jiang, K. S. Novoselov, S. Roth and A. K. Geim, *Phys. Rev. Lett.*, 2006, **97**, 187401–1.
34 A. Gupta, G. Chen, P. Joshi, S. Tadigadapa and P. C. Eklund, *Nano Lett.*, 2006, **6**, 2667–2673.
35 A. C. Ferrari and J. Robertson, *Phys. Rev. B: Condens. Matter Mater. Phys.*, 2000, **61**, 14095–14107.
36 C. Thomsen and S. Reich, *Phys. Rev. Lett.*, 2000, **85**, 5214–5217.
37 F. Tuinstra and J. L. Koenig, *J. Chem. Phys.*, 1970, **53**, 1126.
38 M. Quintana, K. Spyrou, M. Grzelczak, W. R. Browne, P. Rudolf and M. Prato, *ACS Nano*, 2010, **4**, 3527–3533.
39 G. Eda, G. Fanchini and M. Chhowalla, *Nat. Nanotechnol.*, 2008, **3**, 270–274.
40 T. Kuzuba, K. Era, T. Ishii and T. Sato, *Solid State Commun.*, 1978, **25**, 863–865.
41 R. Arenal, A. C. Ferrari, S. Reich, L. Wirtz, J. Y. Mevellec, S. Lefrant, A. Rubio and A. Loiseau, *Nano Lett.*, 2006, **6**, 1812–1816.
42 S. Reich, A. C. Ferrari, R. Arenal, A. Loiseau, I. Bello and J. Robertson, *Phys. Rev. B: Condens. Matter Mater. Phys.*, 2005, **71**, 20520–1.
43 L. Wirtz, M. Lazzeri, F. Mauri and A. Rubio, *Phys. Rev. B: Condens. Matter Mater. Phys.*, 2005, **71**, 241402–1.
44 C. Y. Zhi, Y. Bando, C. C. Tang, D. Golberg, R. G. Xie and T. Sekigushi, *Appl. Phys. Lett.*, 2005, **86**, 213110–1.
45 J. Wu, W. Q. Han, W. Walukiewicz, J. W. Ager, W. Shan, E. E. Haller and A. Zettl, *Nano Lett.*, 2004, **4**, 647–650.

Published on 11 September 2012. Downloaded by Trinity College Dublin on 28/03/2014 12:32:58.